



## OPEN Development of high-dielectric constant polymethyl methacrylate composites doped with tin oxide nanoparticles for advanced electronic applications

Nazeeha S. Alkayal<sup>1</sup>✉, Ali H. Bashal<sup>2</sup>, Talat Habeeb<sup>3</sup> & Abeer S. Elsherbiny<sup>4</sup>

In this study, new polymethyl methacrylate (PMMA) composites were developed by doping with tin oxide (SnO<sub>2</sub>) nanoparticles at varying concentrations (2%, 5%, 10%, and 20% by weight) via solution casting. The dielectric properties and alternating current (AC) conductivity of SnO<sub>2</sub>/PMMA were examined. The impact of SnO<sub>2</sub> ratio, frequency and temperatures on the electrical properties were investigated. Unlike previous studies with limited conditions, our work systematically explores a broad frequency–temperature range, revealing deeper insights into interfacial polarization and charge transport. Results showed that the doping with SnO<sub>2</sub> nanoparticles significantly enhanced the dielectric constant ( $\epsilon'$ ), particularly at lower frequencies, due to increased interfacial polarization (Maxwell-Wagner-Sillars effect). The dielectric loss ( $\epsilon''$ ) also increased with SnO<sub>2</sub> content and temperature, reflecting enhanced interfacial polarization and restricted polymer chain mobility. The AC conductivity followed a power-law dependence on frequency, indicating charge hopping mechanisms, with higher conductivities observed in SnO<sub>2</sub>-doped PMMA. The real and imaginary parts of the electric modulus ( $M'$  and  $M''$ ) increased with nanoparticle content, suggesting improved dielectric relaxation. These results demonstrate that SnO<sub>2</sub> nanoparticles effectively enhance the dielectric and conductive properties of PMMA, making these composites suitable for advanced electronic applications.

**Keywords** Polymethyl methacrylate, Tin oxide nanoparticles, Solution cast method, Dielectric properties, AC conductivity

Dielectric polymer nanocomposites (PNC) are gaining popularity in various fields, including microelectronics, photovoltaics, electromagnetic shielding, optoelectronics, high-performance memory devices, fabrication of high-energy-density capacitors, energy harvester and insulating devices<sup>1–3</sup>. Research suggests that the interface between polymer structures and inorganic nanofillers is crucial in shaping the dielectric behavior of polymeric nanodielectrics (PNDs) across a wide frequency range<sup>4–8</sup>. Adding different types of dopants and fillers to synthesized PNCs can improve their dielectric properties and increase their dielectric values by increasing their concentration. The dielectric constant ( $\epsilon$ ) is a key factor in understanding electrical properties. Large-scale production of nano-dielectrics with enhanced dielectric properties is a significant challenge. Inorganic ceramic fillers reduce the dielectric strength and mechanical properties of polymer composites while increasing  $\epsilon'$  permittivity (and AC conductivity by up to  $10^8$  Scm<sup>-1</sup>) compared to polymer composites without fillers. Additionally, Uniform dispersion of nanoparticles in the polymer matrix improves dielectric properties, with low percolation threshold playing a key role. Extensive research has been conducted in recent years to confirm the dielectric and structural properties of various PNC materials for use as novel polymeric nanodielectrics (PNDs)<sup>9–15</sup>. Polar polymers polyethylene oxide, polyvinyl pyrrolidone, polyvinyl alcohol, polyvinylidene fluoride and PMMA were combined with various inorganic nanofillers (e.g., montmorillonite, silica, alumina, zinc oxide, titanium dioxide and SnO<sub>2</sub>) to create these materials. SnO<sub>2</sub> has multiple applications, including energy storage, chemical sensors, ultra-capacitors, and photovoltaic or AR coatings. It is an n-type semiconductor oxide with

<sup>1</sup>Chemistry Department, Faculty of Science, King Abdulaziz University, Jeddah 21589, Saudi Arabia. <sup>2</sup>Department of Chemistry, Faculty of Science, Taibah University, Yanbu 46423, Saudi Arabia. <sup>3</sup>Department of Biology, Faculty of Science, Taibah University, Yanbu 46423, Saudi Arabia. <sup>4</sup>Department of Chemistry, Faculty of Science, Tanta University, Tanta 31527, Egypt. ✉email: nalkayal@kau.edu.sa

a wide energy band gap of approximately 3.6 eV and a low-cost material<sup>16</sup>. It is commonly combined with polymers to create transparent organic resistive memory devices, gas sensors, transparent solar cell electrodes, electrochromic windows, and energy storage/converter electrolytes<sup>16–19</sup>. PMMA is a versatile polymer known for its optical clarity, mechanical strength, and ease of processing. Despite these advantageous properties, its dielectric performance is inadequate for advanced electronic applications. Enhancing the dielectric properties and AC conductivity of PMMA is essential to broaden its applicability in the field of electronics and optoelectronics. Incorporating inorganic nanoparticles into polymer matrices has emerged as an effective strategy to improve their dielectric properties. Among various nanoparticles, SnO<sub>2</sub> is particularly promising due to its high dielectric constant, good electrical conductivity, and thermal stability. SnO<sub>2</sub> nanoparticles can create additional polarization sites within the polymer matrix, potentially enhancing the dielectric permittivity and reducing the dielectric loss of PMMA. Potentially enhancing the dielectric permittivity and reducing the dielectric loss of PMMA. Previous studies have explored how the incorporation of SnO<sub>2</sub> nanoparticles into different polymers significantly alters their structural, optical, mechanical, and dielectric properties<sup>15,20–22</sup>. Sengwa et al. reported enhanced dielectric properties and tunable band gaps in poly(ethylene oxide) (PEO)/SnO<sub>2</sub> composites<sup>23</sup>. The results showed that dielectric permittivity and electrical conductivity were increased largely at lower frequencies on the dispersion of SnO<sub>2</sub> nanoparticles in the PEO matrix. Also, the direct current (dc) electrical conductivity and chain segmental dynamics have increased nonlinearly as the polymer structure's SnO<sub>2</sub> content has increased. Moreover, two composites of PEO/PMMA blend matrices and oxide nanofillers (SnO<sub>2</sub>) and silica (SiO<sub>2</sub>), in the form of PEO/PMMA/SnO<sub>2</sub> and PEO/PMMA/SiO<sub>2</sub> films were prepared<sup>24</sup>. The broadband radio frequency range (1 MHz to 1 GHz) dielectric permittivity and electrical conductivity of the two films were investigated at ambient temperature. According to the results, these films have low dielectric permittivity values that slightly decrease from 3.4 to 2.8 as the concentration of nanofillers and the applied electric field frequency increase. Recently, thin films of blind PMMA and polyvinylidene fluoride (PVDF) were prepared with and further mixed with SnO<sub>2</sub> nanoparticles in different weight ratios<sup>15</sup>. The structural characterizations showed that the SnO<sub>2</sub> nanoparticles are immiscibly dispersed in the PVDF/PMMA blend matrix, leading to a noticeable rise in the values of dielectric constant and electrical conductivity at constant frequency. Despite these advancements, a comprehensive understanding of the relationship between nanoparticle concentration, dielectric properties, and AC conductivity in PMMA composites is still needed. This study aims to systematically investigate the dielectric properties and AC conductivity of PMMA composites doped with varying concentrations of SnO<sub>2</sub> nanoparticles. The dielectric permittivity, dielectric loss, and AC conductivity of the prepared composites will be measured over a frequency range of 20 Hz to 1 MHz and a temperature range of 25 °C to 120 °C. This study will offer a comprehensive characterization that extends beyond what is typically reported in the literature. Furthermore, Extensive analysis of the Maxwell–Wagner–Sillars (MWS)<sup>25</sup> effect, the power-law frequency dependence of AC conductivity, and the electric modulus have been conducted in the as-prepared SnO<sub>2</sub>/PMMA composite. These investigations provide significant insights into interfacial polarization mechanisms responsible for enhanced dielectric behavior, charge-hopping phenomena, and dielectric relaxation dynamics, which may differ from those observed in other nanoparticle systems reported previously. Thus, this work advances beyond earlier SnO<sub>2</sub>/PMMA studies by systematically covering a broader temperature window, examining higher nanoparticle loadings, and performing detailed electric-modulus analysis, thereby providing new insights into interfacial polarization and dielectric relaxation. Additionally, to the best of our knowledge, the quantitative power-law dependence of AC conductivity has not been comprehensively reported for these composites. In particular, our study covers a wider temperature range (25–120 °C) than most previous reports. Also, it includes higher nanoparticle loadings (up to 20 wt%) than the previous studies. As well as it provides a quantitative frequency-dependent power-law analysis of AC conductivity. These extra parameters clarify the novelty and contextual placement of our study.

## Results and discussion

### Composites characterizations

In the present work, cross-linked SnO<sub>2</sub>(a–d)/PMMA nanocomposites were prepared using an in-situ polymerization with different loadings of SnO<sub>2</sub> NPs. The suggested abbreviations for SnO<sub>2</sub>(a–d)/PMMA nanocomposites of several ratios of SnO<sub>2</sub> NPs are listed in Table S1. Functional groups of PMMA and SnO<sub>2</sub>(a–d)/PMMA nanocomposites were identified using FT-IR spectra as shown in Fig. S2. The spectrum showed the characteristic peaks of PMMA as mentioned by Alkayal<sup>26</sup>. The CH– stretching vibrations of aliphatic and aromatic compounds are attributed to peaks at approximately 2990 and 2940 cm<sup>–1</sup>, respectively. A distinct peak emerged at 1720 cm<sup>–1</sup>, indicating the carbonyl group's stretching vibrations. The C=C stretching vibration of the aromatic rings has a peak around 1490 cm<sup>–1</sup>. The vibration of N–H is linked to the peaks in the absorption range between 3450 and 3370 cm<sup>–1</sup>. Furthermore, the N–H bending exhibits a peak at 1615 cm<sup>–1</sup>, confirming that the amine group of p-phenylenediamine and the carbonyl group of PMMA interact in the cross-linking structure<sup>27</sup>. The interaction between PMMA and SnO<sub>2</sub> nanoparticles was examined by XRD. The XRD diffraction patterns appeared in Fig. S3, and they revealed the amorphous nature of PMMA, and the crystallinity was enhanced with increasing the ratio of SnO<sub>2</sub> as mentioned by Alkayal<sup>26</sup>. The surface morphology of PMMA and SnO<sub>2</sub>(a–d)/PMMA nanocomposites was presented in Fig. S4. SEM image of PMMA shows smoothed holes on the polymer's surface.

After the addition of SnO<sub>2</sub> NPs, the surface morphology changed and became rounded around the micropores. As a result, there is an apparent deformation of the circular hole when a load of SnO<sub>2</sub> increases<sup>26</sup>. The presence of SnO<sub>2</sub> NPs in PMMA was confirmed by EDX measurements, Fig. 1.

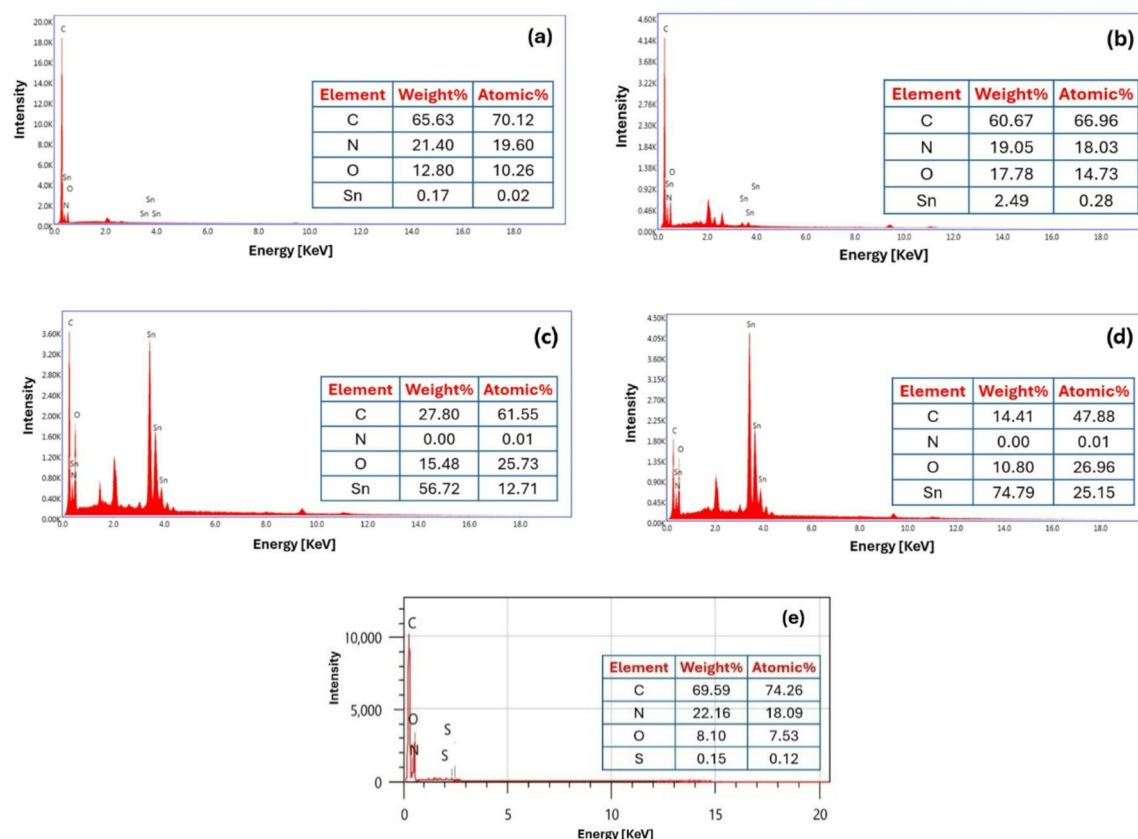


**Fig. 1.** EDX images of: (a) 2% SnO<sub>2</sub>/PMMA, (b) 5% SnO<sub>2</sub>/PMMA, (c) 10% SnO<sub>2</sub>/PMMA (d) 20% SnO<sub>2</sub>/PMMA nanocomposite and (e) PMMA.

## Electrical properties

### Dielectric permittivity

The frequency-dependent permittivity ( $\epsilon'$ ) for PMMA and SnO<sub>2</sub>/PMMA nanoparticles is shown in Fig. 2 at different temperatures at ambient pressure. Clear variation in the electric permittivity is visible within the selected frequency range (approximately < 1 MHz) in Fig. 1. Higher frequencies may induce noise in the signal due to parasitic impedance in the sample holder, and due to the electrode-electrode coupling via the air. The temperature measurement range (25–110 °C), film thickness (~0.2 mm), and electrodes (thin conductive adhesive tape with negligible impedance contribution) are parts of our measurement settings, which use Keysight Impedance analyzer for measuring the dielectric properties. To ensure reproducibility, we assessed the standard deviations from 3 measurement replicas of the dielectric permittivity for PMMA and found it to be around 2.5 on average, which is quite low compared to the average value of around 15 for the permittivity over the frequency range. The same estimate is expected for the remaining samples.

At lower frequencies,  $\epsilon'$  is higher because the dipolar entities within the polymer matrix have sufficient time to align with the applied electric field; as the frequency increases,  $\epsilon'$  gradually decreases and eventually reaches a nearly constant value at higher frequencies. This orientation contributes to the overall polarization, leading to a higher  $\epsilon'$ . For pure PMMA, the intrinsic dipolar relaxation and segmental motions of the polymer chains dominate this polarization. However, in PMMA containing SnO<sub>2</sub> nanoparticles, additional interfacial polarization occurs at the interfaces between the polymer matrix and the nanoparticles. In this case, the Maxwell–Wagner–Sillars effect is prominent, where the accumulation of charges at these interfaces further increases  $\epsilon'$ . As the SnO<sub>2</sub> content increases, the number of such interfaces rises, enhancing the interfacial polarization and thus increasing  $\epsilon'$  compared to pure PMMA. At higher frequencies, the dipolar entities and interfacial charges cannot reorient quickly enough to follow the rapidly oscillating electric field. As a result, the contribution to polarization from these mechanisms diminishes, leading to a decrease in  $\epsilon'$ . Eventually,  $\epsilon'$  reaches a saturation region where the dielectric response is primarily due to electronic polarization, which occurs almost instantaneously and is frequency-independent over the measured range. The observed trends in  $\epsilon'$  are also influenced by temperature. As temperature increases, the mobility of polymer chains and dipolar entities is enhanced, leading to more significant dipolar relaxation and interfacial polarization effects at lower frequencies.

This increased mobility also means that the transition from high  $\epsilon'$  at low frequencies to saturated  $\epsilon'$  at high frequencies occurs more rapidly. The impact of SnO<sub>2</sub> nanoparticles becomes more pronounced at elevated temperatures due to enhanced interfacial polarization and restricted polymer chain mobility near the nanoparticles, which further contributes to the overall permittivity. It is worth noting that the absolute values of

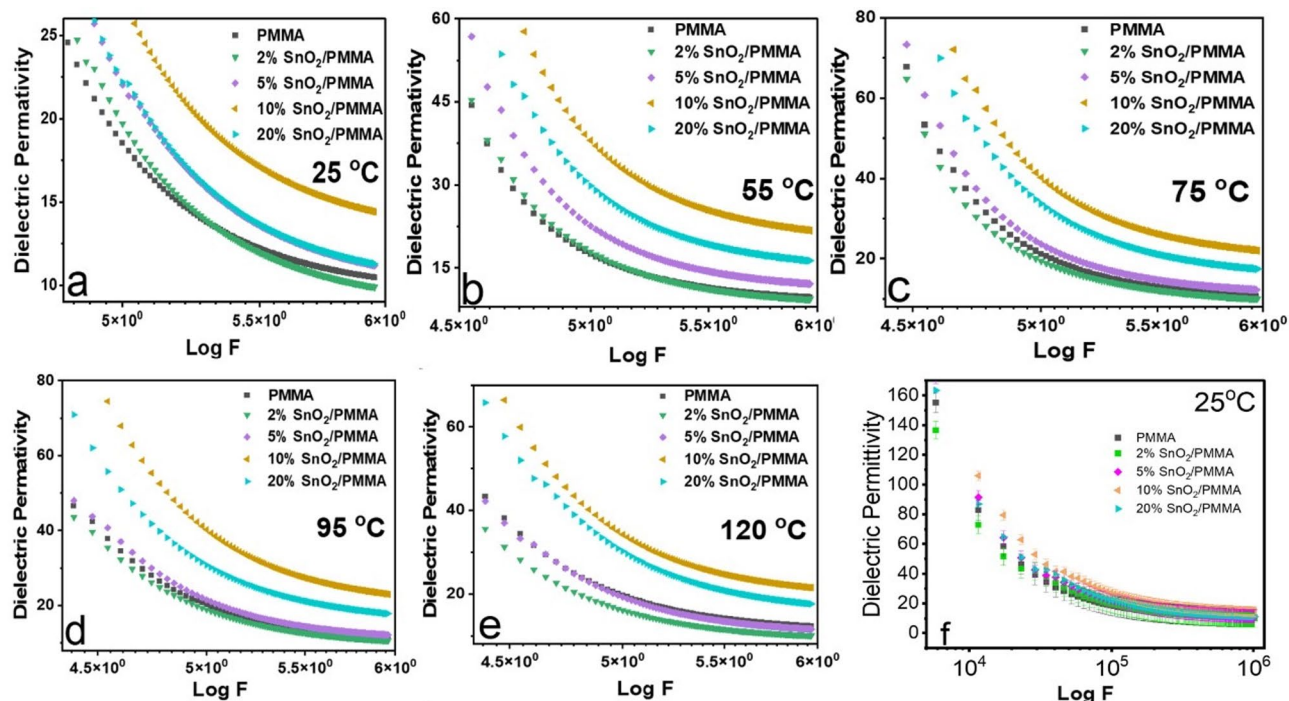


**Fig. 2.** Changes in the permittivity of PMMA and X%SnO<sub>2</sub>/PMMA samples at different frequencies at (a) 25 °C, (b) 55 °C, (c) 75 °C, (d) 95 °C, and (e) 120 °C and (f) error bar.

the calculated permittivity may differ from those reported in the literature. This discrepancy can be attributed, in part, to uncertainties in the measurement of the sample geometry (thickness and area in Eq. (1)), which directly influence the calculated permittivity values from impedance data.

#### Dielectric loss

In Fig. 3, the dielectric loss as a function of frequency is illustrated for PMMA and X%SnO<sub>2</sub>/PMMA across various temperatures. The behavior of  $\epsilon''$  of the PMMA and SnO<sub>2</sub>-containing PMMA as a function of frequency and temperature can be understood by considering the effects of temperature and nanoparticle content on dielectric losses. At the low temperature of 25 °C,  $\epsilon''$  is highest for pure PMMA. This can be attributed to the intrinsic dipolar relaxation processes within the polymer matrix, where pure PMMA exhibits significant dielectric loss due to its dipolar entities and chain segmental motions. As the temperature increases, the dielectric losses ( $\epsilon''$ ) show a different trend, approximately increasing with the SnO<sub>2</sub> concentration. Higher temperatures provide more thermal energy, which enhances the mobility of polymer chains and the activity of dipolar entities. In SnO<sub>2</sub>-containing PMMA, the introduction of nanoparticles creates additional interfaces within the polymer matrix. These interfaces lead to enhanced interfacial polarization (Maxwell–Wagner–Sillars effect), which becomes more significant at higher temperatures and with higher SnO<sub>2</sub> content. The nanoparticles restrict the mobility of polymer chains near their surfaces, and this constrained region responds differently to the applied electric field, contributing to increased dielectric losses. Moreover, as the temperature rises, the increased thermal energy facilitates ionic and electronic conductivity within the polymer matrix. SnO<sub>2</sub> nanoparticles can enhance this conductivity by providing pathways for charge carriers, further contributing to dielectric losses. Thus, with increasing temperature, the dielectric losses in SnO<sub>2</sub>-containing PMMA increase more significantly compared to pure PMMA due to enhanced interfacial polarization, restricted chain mobility near nanoparticles, and increased conductivity losses. This results in the observed trend where  $\epsilon''$  approximately increases with the SnO<sub>2</sub> concentration as the temperature rises.

#### AC conductivity

The variation of the frequency-dependent conductivity with SnO<sub>2</sub> content is shown in Fig. 4 and somewhat resembles that observed for  $\epsilon''$  in Fig. 2. For instance, at 25 °C, the conductivity is highest for pure PMMA. This can be attributed to the intrinsic ionic and electronic conduction mechanisms within the pure polymer matrix. At this low temperature, the dipolar relaxation processes and segmental motions of the polymer chains contribute significantly to the dielectric loss and, consequently, to the conductivity. Pure PMMA, without the restrictive influence of nanoparticles, exhibits a higher intrinsic conductivity due to the greater mobility of its polymer chains and dipolar entities. As the temperature increases, the conductivity of SnO<sub>2</sub>-containing PMMA increases more significantly compared to pure PMMA. This increase can be explained by several factors. Firstly, the introduction of SnO<sub>2</sub> nanoparticles creates additional interfaces within the polymer matrix. These interfaces enhance interfacial polarization (Maxwell–Wagner–Sillars effect), which contributes to both the dielectric loss

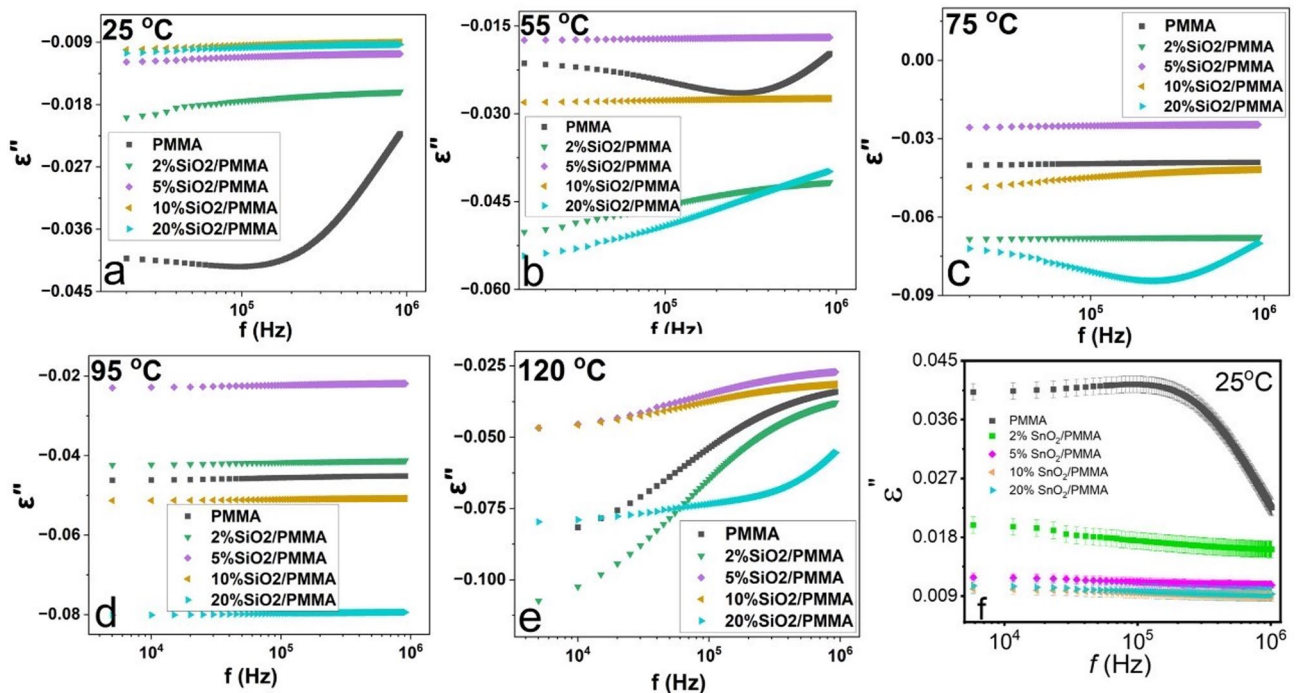


**Fig. 3.** Changes in the loss of PMMA and X%SnO<sub>2</sub>/PMMA samples at different frequencies at (a) 25 °C, (b) 55 °C, (c) 75 °C, (d) 95 °C, and (e) 120 °C and (f) error bar.

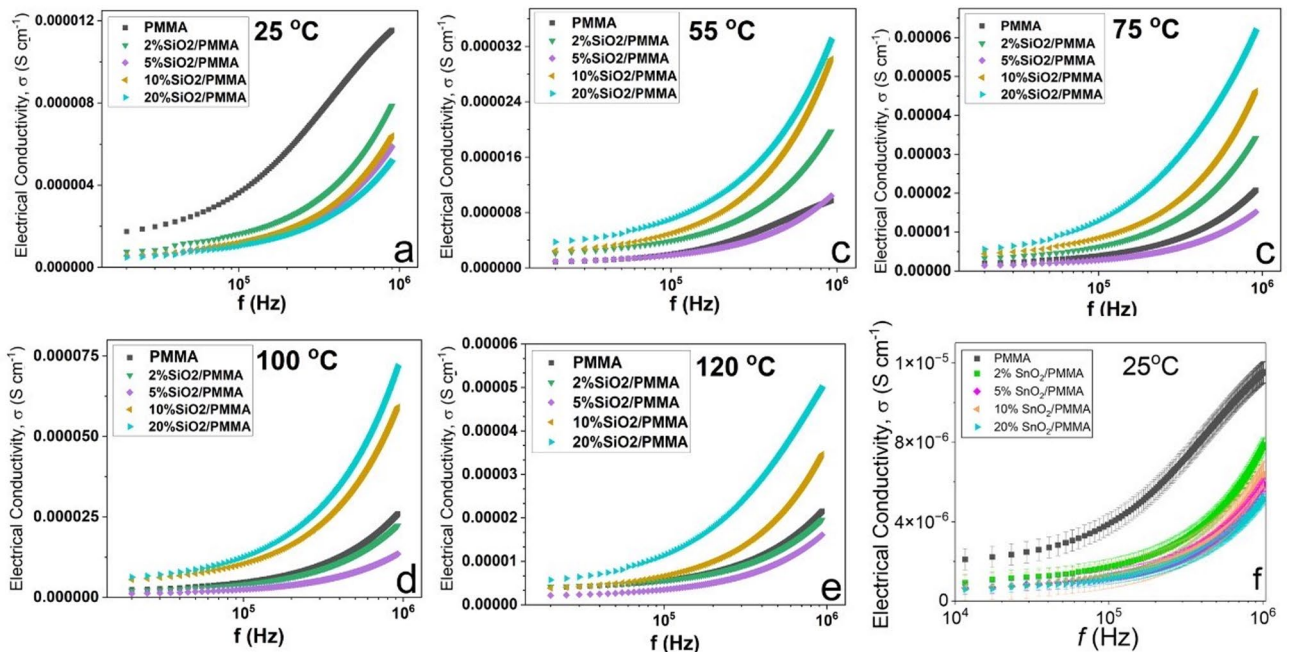


**Fig. 4.** Changes in the loss of PMMA and X%SnO<sub>2</sub>/PMMA samples at different frequencies at (a) 25 °C, (b) 55 °C, (c) 75 °C, (d) 95 °C, and (e) 120 °C and (f) error bar.

( $\epsilon''$ ) and the conductivity. At higher temperatures, the thermal energy increases the mobility of polymer chains and dipolar entities, leading to enhanced dipolar relaxation and interfacial polarization, especially in SnO<sub>2</sub>-containing PMMA. Secondly, SnO<sub>2</sub> nanoparticles introduce regions where polymer chain mobility is restricted. This restriction can create localized areas of higher charge carrier concentration, enhancing the overall conductivity as temperature rises. Additionally, the nanoparticles can facilitate pathways for ionic and electronic charge carriers, further contributing to the increase in conductivity with higher SnO<sub>2</sub> content. Conductivity

follows a power law dependence on the frequency, given by  $\sigma(\omega) \propto \omega^n$ , where the exponent  $n$  is larger than 1. This type of power law dependence indicates that the conduction mechanism is dominated by the hopping or tunneling of charge carriers between localized states. The exponent larger than 1 suggests that the charge transport is highly dispersive, implying a significant interaction between the charge carriers and the dynamic matrix, which in this case is influenced by the presence of SnO<sub>2</sub> nanoparticles. The power law also suggests that the interfacial polarization and relaxation processes are significant contributors to the overall dielectric and conductive properties. At higher frequencies, the increased energy availability facilitates these hopping processes, leading to the observed frequency-dependent conductivity.

At this point, it is worth emphasizing briefly some key results at selected temperature and frequency. Table 1 summarizes  $\epsilon'$ ,  $\epsilon''$ ,  $\sigma_{ac}$  and the high-frequency power-law exponent  $s$  for all samples at  $f=1$  MHz and  $T \approx 95$  °C. Dielectric constant and loss increase systematically with SnO<sub>2</sub> loading while  $\sigma_{ac}$  also rises, showing enhanced interfacial polarization and more efficient charge pathways in doped composites. The exponent  $s$  grows from  $\sim 0.70$  (pure PMMA) to  $\sim 0.90$  (20% SnO<sub>2</sub>), indicating progressively more dispersive, hopping-dominated charge transport as nanoparticle content increases. These observations are consistent with the manuscript's interpretation that Maxwell–Wagner–Sillars interfacial polarization and nanoparticle-assisted hopping govern the enhanced dielectric and conductive behavior. The marked conductivity increase at high loadings suggests approaching percolation; electrical leakage and thermal stability should be evaluated when SnO<sub>2</sub> content exceeds the optimized threshold.

An illustrative energy-density estimate using  $U = \frac{1}{2}\epsilon_r\epsilon_0 E^2$  and literature PMMA breakdown fields  $E \sim 80$ – $120$  kV mm<sup>-1</sup> indicates a rise from  $\sim 0.17$  to  $0.38$  J cm<sup>-3</sup> for ideal PMMA ( $\epsilon \approx 6$ ) to  $\sim 1.56$ – $3.51$  J cm<sup>-3</sup> for 20 wt% SnO<sub>2</sub>/PMMA ( $\epsilon \approx 55$ ) at 1 MHz and  $\sim 100$  °C (Table 1), assuming the same  $E$  for comparison. Since breakdown strength was not measured here and can decrease in filled systems, these values are indicative; device-level measurements of  $E_{BD}$ , leakage, and cycling stability will be essential for application-level benchmarking. We also note that  $\epsilon''$  increases at higher temperature and loading, reflecting interfacial polarization and conduction contributions; mitigating strategies include hybrid/core–shell oxides, surface functionalization, optimized loading, and multilayer designs.

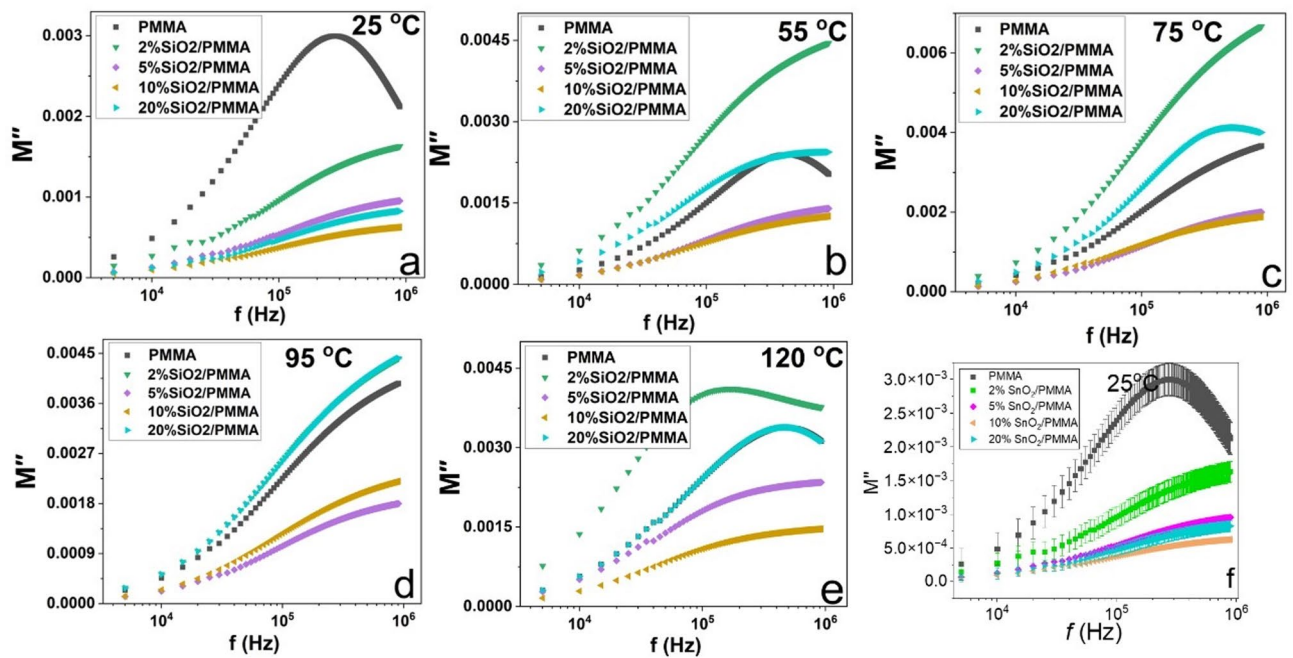
#### Electric modulus

Figure 5 shows the frequency-dependent imaginary part of the complex electric modulus  $M''$  at different temperatures for pure and SnO<sub>2</sub>-contained PMMA.  $M''$  tends to peak at higher frequencies at higher temperatures. This is a general trend for most of the samples and may be associated with the emergence of the dielectric relaxation processes in the samples.  $M''$  peak also tends to decrease with increasing concentration of SnO<sub>2</sub>, apart from a mismatch at some concentrations, such as 2% and 20%. The dielectric relaxation of the PMMA is due to the polarization of its functional group as well as the charge accumulation at the polymer segment–segment interface. The latter gives rise to the known Maxwell–Wagner polarization. These polymer-type polarizations mix with those associated with SnO<sub>2</sub> structures, which may explain the broadening of the frequency-dependent profile for SnO<sub>2</sub>/PMMA as compared to the pure PMMA for most of the temperatures. For PMMA with increasing SnO<sub>2</sub> nanoparticle content, the increase in the real dielectric modulus ( $M'$ ) at the high-frequency saturation region (Fig. 6) can be attributed to the fact that the introduction of SnO<sub>2</sub> nanoparticles enhances interfacial polarization due to the Maxwell–Wagner–Sillars effect. This effect becomes more pronounced with higher nanoparticle content, contributing significantly to the dielectric response. Additionally, the presence of SnO<sub>2</sub> nanoparticles restricts the mobility of PMMA chains near the nanoparticle surfaces. This restriction affects the segmental motion of the polymer chains, particularly at high frequencies where the dielectric response is sensitive to fast dipolar relaxation processes. Moreover, as the SnO<sub>2</sub> nanoparticle content increases, the total interfacial area between the PMMA matrix and the nanoparticles increases, enhancing polarization effects due to interactions at these interfaces. The SnO<sub>2</sub> nanoparticles may also introduce additional dipolar entities or influence existing dipolar groups in PMMA, contributing to the dielectric modulus, especially at high frequencies where dipolar relaxation processes are significant.

Furthermore, at higher SnO<sub>2</sub> concentrations, the formation of a percolative network might occur, further enhancing the dielectric properties by improving connectivity and polarization effects. These combined factors result in an increased real dielectric modulus ( $M'$ ) in the high-frequency saturation region with increasing SnO<sub>2</sub> nanoparticle content in PMMA. The real ( $M'$ ) and imaginary ( $M''$ ) parts of the electric modulus were analyzed to gain insights into the dielectric relaxation behavior of the composites. The results showed that both  $M'$  and  $M''$  increased with SnO<sub>2</sub> content, indicating improved dielectric relaxation dynamics. This enhancement is due to the presence of SnO<sub>2</sub> nanoparticles, which interact with the PMMA matrix and alter its dielectric properties.

Sample	$\epsilon'$	$\epsilon''$	AC conductivity, $\sigma_{ac}$ ( $\times 10^{-6}$ S)	Power law exponent
PMMA	6.0 ± 1.0	0.025 ± 0.005	1.0 ± 0.2	0.70
2% SnO <sub>2</sub> /PMMA	12.0 ± 1.5	0.030 ± 0.006	2.0 ± 0.3	0.75
5% SnO <sub>2</sub> /PMMA	18.0 ± 2.0	0.035 ± 0.007	3.0 ± 0.4	0.78
10% SnO <sub>2</sub> /PMMA	30.0 ± 3.0	0.050 ± 0.008	5.0 ± 0.6	0.85
20% SnO <sub>2</sub> /PMMA	55.0 ± 5.0	0.070 ± 0.010	7.2 ± 0.8	0.90

**Table 1.** Summary of key values  $\epsilon'$ ,  $\epsilon''$ , AC conductivity, and the power-law exponent, at 1 MHz and  $\sim 100$  °C for the PMMA samples.



**Fig. 5.** illustrates the changes in the imaginary part of the electric modulus for the samples at different frequencies and temperatures: (a) 25 °C, (b) 55 °C, (c) 75 °C, (d) 95 °C, (e) 120 °C and (f) error bar.

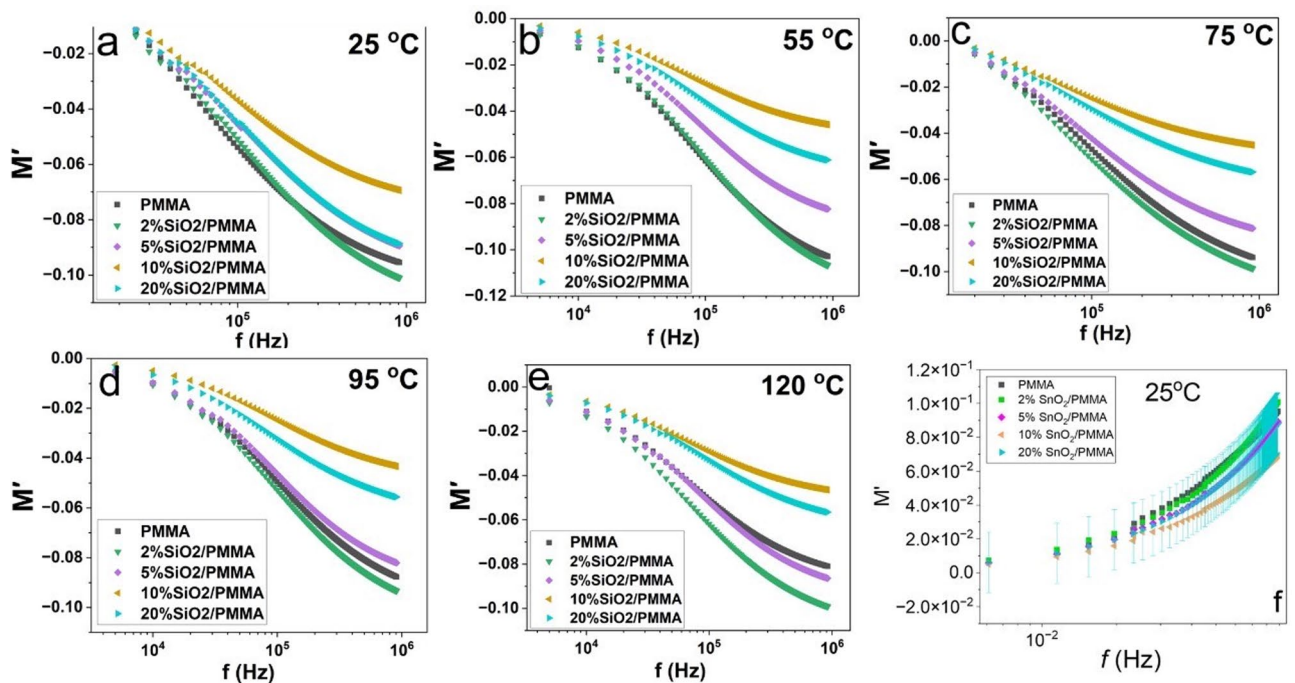


**Fig. 6.** Illustrates the changes in the real part of the electric modulus for the samples at different frequencies and temperatures: (a) 25 °C, (b) 55 °C, (c) 75 °C, (d) 95 °C, (e) 120 °C and (f) error bar.

Additionally, the broad, asymmetric nature of the  $M''$  peaks across compositions suggests a distribution of relaxation times rather than a single well-defined relaxation event. This dispersion likely originates from structural heterogeneity within the nanocomposites, where variations in local microenvironments near nanoparticle interfaces lead to multiple relaxation pathways. The shift of  $M''$  maxima toward higher frequencies with increasing temperature further reflects thermally assisted charge migration and short-range hopping. Together, these features confirm that the relaxation process in  $\text{SnO}_2/\text{PMMA}$  composites is dominated by

interfacial polarization and localized carrier dynamics rather than long-range translational motion, in agreement with the observed trends in  $\epsilon''$  and  $\sigma_a$ .

## Conclusion

This study demonstrates that the addition of SnO<sub>2</sub> nanoparticles significantly enhances the dielectric and conductive properties of PMMA. The dielectric constant ( $\epsilon'$ ) showed a marked improvement, especially at low frequencies, due to increased interfacial polarization resulting from the Maxwell-Wagner-Sillars effect. Furthermore, the dielectric loss ( $\epsilon''$ ) increased with both temperature and SnO<sub>2</sub> concentration, reflecting the role of the nanoparticles in restricting polymer chain mobility and enhancing charge accumulation at the interfaces. The frequency-dependent AC conductivity followed a power-law behavior, indicative of charge carrier hopping mechanisms, with SnO<sub>2</sub>-doped PMMA composites exhibiting higher conductivity than pure PMMA. These findings suggest that the incorporation of SnO<sub>2</sub> nanoparticles not only improves the dielectric relaxation dynamics but also enhances the overall electrical performance of PMMA, making these composites highly suitable for various electronic applications, such as energy storage, sensors, and transducers. Moreover, the real ( $M'$ ) and imaginary ( $M''$ ) parts of the electric modulus exhibited significant enhancements in the doped composites, further corroborating the increased polarization effects. As the concentration of SnO<sub>2</sub> nanoparticles increased, the interfacial area between the PMMA matrix and the nanoparticles expanded, leading to a more pronounced dielectric response. The results indicate that optimizing the SnO<sub>2</sub> concentration can tailor the electrical properties of PMMA composites for specific uses. Particularly, the observed dielectric enhancement and increased  $\sigma_{ac}$  imply improved energy-storage capability and faster charge/discharge response in devices. Higher  $\epsilon'$  at low frequency raises the potential stored energy density for capacitor applications. Moving forward, exploring other types of nanoparticles or hybrid composites, as well as investigating their behavior under different environmental conditions, could unlock new potentials for advanced technological applications, especially in areas requiring high-performance dielectric materials.

## Experimental

### Materials

PMMA of molecular weight of 300 K was employed as a starting polymer and obtained from Alfa Aesar by Thermos Fisher, Erlenbachweg, Germany. SnO<sub>2</sub> nanoparticles of particle size less than 100 nm were provided from Nano Gate CO, Cairo, Egypt. Tetrahydrofuran (THF; 99.5%) was purchased from Fisher Chemical, Loughborough, UK, and p-phenylenediamine (p-PDA) (C<sub>6</sub>H<sub>4</sub>NH<sub>2</sub>)<sub>2</sub>; Fluka, Loughborough, UK, and the chemicals were used without purification or treatment. Cr(NO<sub>3</sub>)<sub>3</sub>·9H<sub>2</sub>O (97%) was provided by Panreac, Milano, Italy. HCl (35%) supplied from LOBA Chemie, Mumbai, India and used without any further purifications.

### SnO<sub>2</sub>/PMMA nanocomposite film Preparation

SnO<sub>2</sub>/PMMA nanocomposites were synthesized via a polycondensation process following the method described in reference<sup>26</sup> and Fig. S1. 1.0 g of poly (methyl methacrylate) (PMMA) was completely dissolved in 50 mL of tetrahydrofuran (THF) under magnetic stirring (400 rpm) at room temperature for 30 min to obtain a homogeneous polymer solution. Subsequently, different ratios of SnO<sub>2</sub> nanoparticles 2, 5, 10, and 20 wt% were added into the PMMA solution. The resulting dispersions were sonicated for 10 min using an ultrasonic bath to ensure uniform nanoparticle distribution. 0.2 g of p-phenylenediamine (p-PDA) was added as a cross-linking agent and the mixture was refluxed at 70 °C for 6 h with continuous stirring at 400 rpm to promote the crosslinking and polycondensation reaction between PMMA and p-PDA in the presence of SnO<sub>2</sub>. The obtained reaction mixture was poured into clean Petri dishes and allowed to dry at room temperature (25 °C) for 24 h to facilitate solvent evaporation and film formation. The as-formed films were then post-dried in a vacuum oven at 50 °C for 12 h to remove any residual THF and complete curing.

### Characterization techniques

Fourier-Transform Infrared (FT-IR) spectra of the nanocomposite were captured using potassium bromide discs by a Nicolet Magna 6700 FT spectrometer (Cambridge, UK) in the range of 600–4000 cm<sup>-1</sup>. X-ray diffraction (XRD) patterns were studied using a Philips diffractometer (Model: X'Pert-Pro MPD; Philips, now PAN a typical, Malvern, Worcestershire, United Kingdom) with Cu K $\alpha$  radiation (wavelength 1.5418 Å) at 40 kV and 40 mA. The patterns were collected between 2 $\theta$  of 5° and 60°, and the scan speed was 1.5°/min. Scanning electron microscopy (SEM) imaging was performed with an FEI TENE0 VS microscope equipped with an EDAX detector. The polymer sample was affixed to an aluminum stub using adhesive carbon tape and coated with a 3 nm layer of Iridium through sputtering. This was done to prevent the sample from accumulating electric charges during imaging. The dielectric properties and electrical conductivity for all samples were explored within the temperature range of 25–120 °C and the frequency range of 20 Hz to 1 MHz, with an AC amplitude of 0.5 V and zero DC voltage. The “Keysight E4990A-02” instrument was utilized to measure the impedance spectra of our samples, which were in the form of circular films with approximately 1 mm thickness and a radius of approximately 0.5 cm. To measure the temperature, a mercury bulb thermometer was used, ensuring close contact with the surface of the pellets positioned on a hot plate equipped with a temperature controller. The dielectric permittivity ( $\epsilon'$ ) was calculated by using Eq. (1).

$$\epsilon' = Cd/\epsilon_0 A \quad (1)$$

where C is the capacitance of the sample-filled capacitor, d is the sample thickness,  $\epsilon_0$  is the vacuum permittivity and A is the electrode area. The capacitance is calculated from the measured impedance data using the

relationship  $C = \frac{Z''}{\omega(Z'^2 + Z''^2)}$ , where  $\omega$  is the angular frequency and  $Z'$  and  $Z''$  are, respectively, the real part and the imaginary part of the measured impedance by the Keysight instrument.

The electric modulus  $M^*$  (consisting of real and imaginary parts) was measured as a function of the dielectric permittivity and dielectric loss using Eq. 2.

$$M^* = M' + iM'' \quad (2)$$

Where the real component of the electric modulus  $M$  is measured using the equation

$$M' = \frac{\epsilon'}{\epsilon'^2 + \epsilon''^2}$$

and

$$M'' = \frac{\epsilon''}{\epsilon'^2 + \epsilon''^2}$$

The ac conductivity ( $\sigma_{ac}$ ) is calculated as a function of frequency by using Eq. 3.

$$\sigma_{ac} = \frac{d}{A} \frac{Z'}{(Z'^2 + Z''^2)} \quad (3)$$

Copper tapes were used as the electrodes that were fixed at the films with a thin layer of adhesive (with a negligible contribution to the impedance) to avoid using a conducting paste (available to us was a silver paste) that would diffuse into the sample, resulting in an unwanted signal in the impedance spectrum. The adhesive layer is partially conductive and very thin, lowering its resistance and capacitive reactance. Thus, this layer has a negligible contribution to the sample's measured impedance.

## Data availability

Data is provided within the manuscript or supplementary information files.

Received: 15 September 2025; Accepted: 27 November 2025

Published online: 05 December 2025

## References

- Daniel, T. & Patricia, I. in *Advances in Ceramics* (ed Costas Sikalidis) Ch. 7 (IntechOpen, 2011).
- Mittal, V. In-situ synthesis of polymer nanocomposites. In *In-situ Synthesis of Polymer Nanocomposites* 1–25 (2011).
- Abdel-Aal, S. K., Kandeel, M. F., El-Sherif, A. F. & Abdel-Rahman, A. S. Synthesis, Characterization, and optical properties of new Organic-Inorganic hybrid perovskites  $[(NH_3)_2(CH_2)_3]CuCl_4$  and  $[(NH_3)_2(CH_2)_4]CuCl_2Br_2$ . *Phys. Status Solidi (a)*. **218**, 2100036. <https://doi.org/10.1002/pssa.202100036> (2021).
- Tanaka, T. & Vaughan, A. S. *Tailoring of Nanocomposite Dielectrics: From Fundamentals to Devices and Applications* (Jenny Stanford Publishing, Singapore 2016).
- Tsonos, C. et al. Polyvinylidene fluoride/magnetite nanocomposites: Dielectric and thermal response. *J. Phys. Chem. Solids* **129**, 378–386 (2019).
- Tsonos, C. et al. Electromagnetic wave absorption properties of ternary poly (vinylidene fluoride)/magnetite nanocomposites with carbon nanotubes and graphene. *RSC Adv.* **6**, 1919–1924 (2016).
- Singh, P. K. et al. Effect of interface in dielectric relaxation properties of PEMA–BaZrO<sub>3</sub> nanocomposites. *Polym. Bull.* **75**, 4003–4018 (2018).
- Alhabill, F. N., Ayoob, R., Andritsch, T. & Vaughan, A. S. Introducing particle interphase model for describing the electrical behaviour of nanodielectrics. *Mater. Design.* **158**, 62–73 (2018).
- Sengwa, R. J., Choudhary, S. & Dhatarwal, P. Nonlinear optical and dielectric properties of TiO<sub>2</sub> nanoparticles incorporated PEO/PVP blend matrix based multifunctional polymer nanocomposites. *J. Mater. Sci. Mater. Electron.* **30**, 12275–12294 (2019).
- Choudhary, S. & Sengwa, R. ZnO nanoparticles dispersed PVA–PVP blend matrix based high performance flexible nanodielectrics for multifunctional microelectronic devices. *Curr. Appl. Phys.* **18**, 1041–1058 (2018).
- Sengwa, R. J. & Choudhary, S. Dielectric and electrical properties of PEO–Al<sub>2</sub>O<sub>3</sub> nanocomposites. *J. Alloys Compd.* **701**, 652–659 (2017).
- Sengwa, R., Choudhary, S. & Dhatarwal, P. Investigation of alumina nanofiller impact on the structural and dielectric properties of PEO/PMMA blend matrix-based polymer nanocomposites. *Adv. Compos. Hybrid. Mater.* **2**, 162–175 (2019).
- Dhatarwal, P. & Sengwa, R. Impact of PVDF/PEO blend composition on the  $\beta$ -phase crystallization and dielectric properties of silica nanoparticles incorporated polymer nanocomposites. *J. Polym. Res.* **26**, 196 (2019).
- Dhatarwal, P., Choudhary, S. & Sengwa, R. Significantly enhanced dielectric properties and chain segmental dynamics of PEO/SnO<sub>2</sub> nanocomposites. *Polym. Bull.* **78**, 2357–2373 (2021).
- Bafna, M. et al. Study of structural and dielectric properties of blended poly (vinylidene fluoride) and poly (methyl methacrylate) multifunctional nanocomposites doped with nano-SnO<sub>2</sub>. *J. Mater. Sci. Mater. Electron.* **35**, 494 (2024).
- Orlandi, M. O. *Tin Oxide Materials: Synthesis, properties, and Applications* (Elsevier, Amsterdam 2019).
- Sarkar, P. K., Bhattacharjee, S., Prajapat, M. & Roy, A. Incorporation of SnO<sub>2</sub> nanoparticles in PMMA for performance enhancement of a transparent organic resistive memory device. *RSC Adv.* **5**, 105661–105667 (2015).
- Kar, E. et al. 2D SnO<sub>2</sub> nanosheet/PVDF composite based flexible, self-cleaning piezoelectric energy harvester. *Energy. Conv. Manag.* **184**, 600–608 (2019).
- Channu, V. S. R., Rambabu, B., Kumari, K., Kalluru, R. R. & Holze, R. SnO<sub>2</sub>/PANI nanocomposite electrodes for supercapacitors and lithium ion batteries. *Electrochem. Energy Technol.* **4**, 32–38 (2018).
- Deeba, F., Gupta, A. K., Kulshrestha, V., Bafna, M. & Jain, A. Analysing the dielectric properties of ZnO doped PVDF/PMMA blend composite. *J. Mater. Sci. Mater. Electron.* **33**, 23703–23713 (2022).
- Anu, M. & Pillai, S. S. Structure, thermal, optical and dielectric properties of SnO<sub>2</sub> nanoparticles-filled HDPE polymer. *Solid State Commun.* **341**, 114577 (2022).

22. Dhatarwal, P. & Sengwa, R. Tunable  $\beta$ -phase crystals, degree of crystallinity, and dielectric properties of three-phase PVDF/PEO/SiO<sub>2</sub> hybrid polymer nanocomposites. *Mater. Res. Bull.* **129**, 110901 (2020).
23. Sengwa, R. & Dhatarwal, P. Polymer nanocomposites comprising PMMA matrix and ZnO, SnO<sub>2</sub>, and TiO<sub>2</sub> nanofillers: a comparative study of structural, optical, and dielectric properties for multifunctional technological applications. *Opt. Mater.* **113**, 110837 (2021).
24. Dhatarwal, P., Sengwa, R. J. & Choudhary, S. Broadband radio frequency dielectric permittivity and electrical conductivity of dispersed tin oxide and silica nanoparticles in poly(ethylene oxide)/poly(methyl methacrylate) blend matrix-based nanocomposites for nanodielectric applications. *J. Macromol. Sci. Part. B.* **61**, 111–120. <https://doi.org/10.1080/00222348.2021.1971839> (2022).
25. Khodadadi, S. & Sokolov, A. P. Protein dynamics: From rattling in a cage to structural relaxation. *Soft Matter.* **11**, 4984–4998 (2015).
26. Alkayal, N. S. Fabrication of cross-linked PMMA/SnO<sub>2</sub> nanocomposites for highly efficient removal of chromium (III) from wastewater. *Polymers* **14**, 2101 (2022).
27. Alkayal, N. S., Altowairki, H., Alosaimi, A. M. & Hussein, M. A. Network template-based cross-linked poly(methyl methacrylate)/tin(IV) oxide nanocomposites for the photocatalytic degradation of MB under UV irradiation. *J. Mater. Res. Technol.* **18**, 2721–2734. <https://doi.org/10.1016/j.jmrt.2022.03.133> (2022).

## Acknowledgements

This project was funded by the Deanship of Scientific Research (DSR) at King Abdulaziz University (KAU), Jeddah, Saudi Arabia under Grant No. (IPP: 224-247-2025). Therefore, the author gratefully acknowledges with thanks DSR for technical and financial support.

## Author contributions

Nazeeha S. Alkayal, Ali H. Bashal, Talat Habeeb, and Abeer S. Elsherbiny: validation; Nazeeha S. Alkayal, Ali H. Bashal, and Talat Habeeb: formal analysis; Nazeeha S. Alkayal, Ali H. Bashal and Talat Habeeb: investigation and data curation; Ali H. Bashal, Talat Habeeb, Nazeeha S. Alkayal and Abeer S. Elsherbiny: writing-original draft preparation; Nazeeha S. Alkayal, Ali H. Bashal, Talat Habeeb, and Abeer S. Elsherbiny: review and editing; Nazeeha S. Alkayal, Ali H. Bashal, Talat Habeeb, and Abeer S. Elsherbiny: final revision.

## Declarations

### Competing interests

The authors declare no competing interests.

### Consent to participate

All the authors agreed to participate in this work.

### Additional information

**Supplementary Information** The online version contains supplementary material available at <https://doi.org/10.1038/s41598-025-30922-5>.

**Correspondence** and requests for materials should be addressed to N.S.A.

**Reprints and permissions information** is available at [www.nature.com/reprints](http://www.nature.com/reprints).

**Publisher's note** Springer Nature remains neutral with regard to jurisdictional claims in published maps and institutional affiliations.

**Open Access** This article is licensed under a Creative Commons Attribution-NonCommercial-NoDerivatives 4.0 International License, which permits any non-commercial use, sharing, distribution and reproduction in any medium or format, as long as you give appropriate credit to the original author(s) and the source, provide a link to the Creative Commons licence, and indicate if you modified the licensed material. You do not have permission under this licence to share adapted material derived from this article or parts of it. The images or other third party material in this article are included in the article's Creative Commons licence, unless indicated otherwise in a credit line to the material. If material is not included in the article's Creative Commons licence and your intended use is not permitted by statutory regulation or exceeds the permitted use, you will need to obtain permission directly from the copyright holder. To view a copy of this licence, visit <http://creativecommons.org/licenses/by-nc-nd/4.0/>.

© The Author(s) 2025